Supporting Information for

Lithium Growth on Alloying Substrates and the Effect on Volumetric Expansion

Laura C. Merrill[1]*, Robert C. Craig[2], Damion P. Cummings[2], Julia L. Deitz[2]

1. Nanoscale Sciences Department, Sandia National Laboratories, Albuquerque, NM, 87123, USA

2. Materials Characterization and Performance, Sandia National Laboratories, Albuquerque, NM, 87123, USA

*Corresponding author: Laura Merrill, lcmerri@sandia.gov

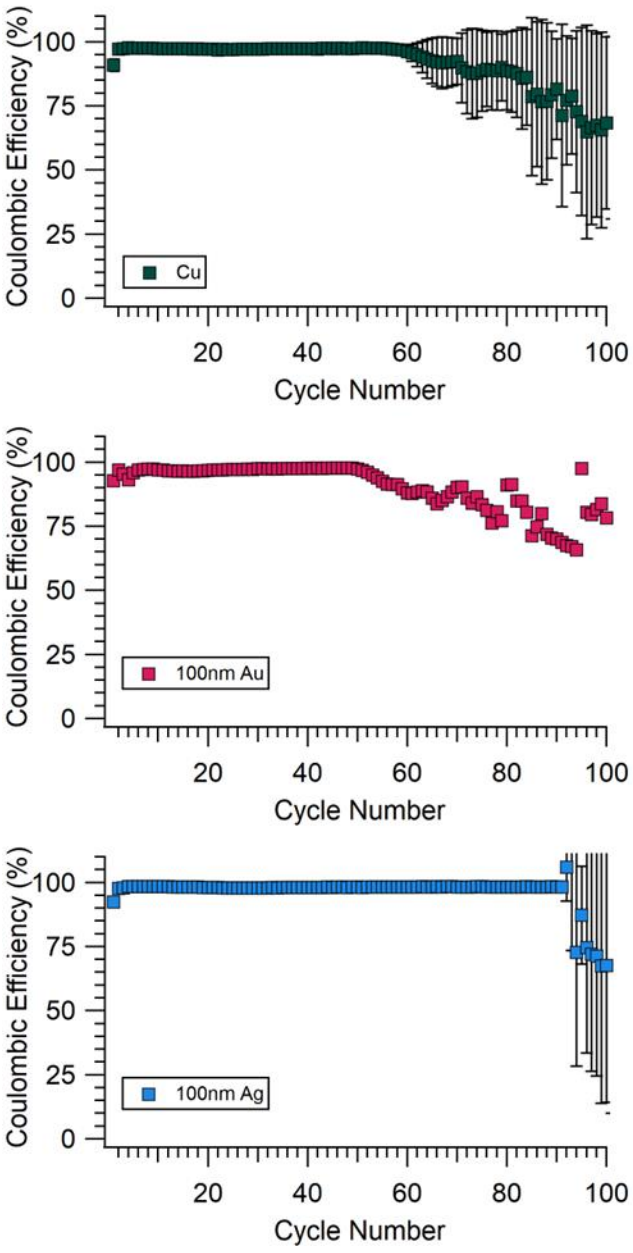


Figure S1: Extended cycling for Li on Cu (top), 100 nm Au (middle), and 100 nm Ag (bottom) substrates in 1 M LiTFSI in DOL:DME with 5 wt% $LiNO_3$. Averages are representative of at least 3 cells with error bars representing the standard deviation. Cells were cycled at 1 mA/cm^2 for 1 mAh/cm^2.

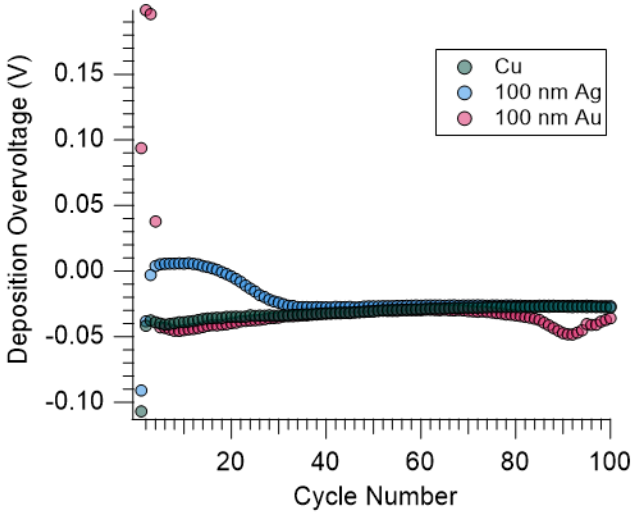


Figure S2: Deposition overvoltage vs cycle number from representative coin cells from Figure 1 and Figure S1. Deposition overvoltage was taken from the voltage when current is first applied on each cycle.

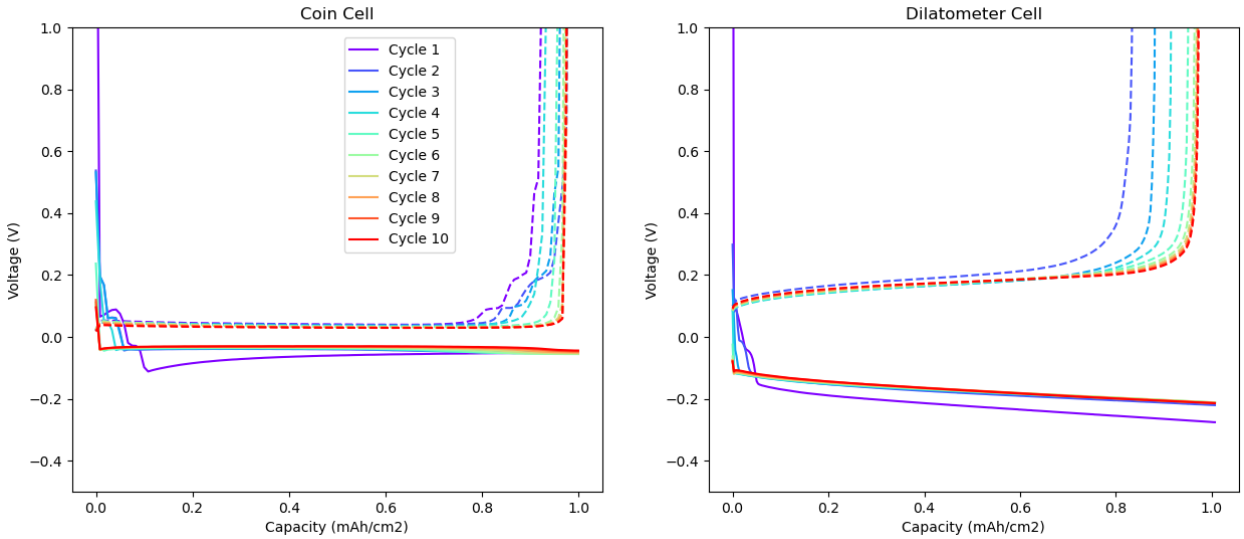


Figure S3: Voltage vs. capacity curves for the first 10 cycles of Li cycling on 100 nm Au at 1 mA/cm^2 for 1 mAh/cm^2 in (left) a coin cell and (right) a dilatometer cell.

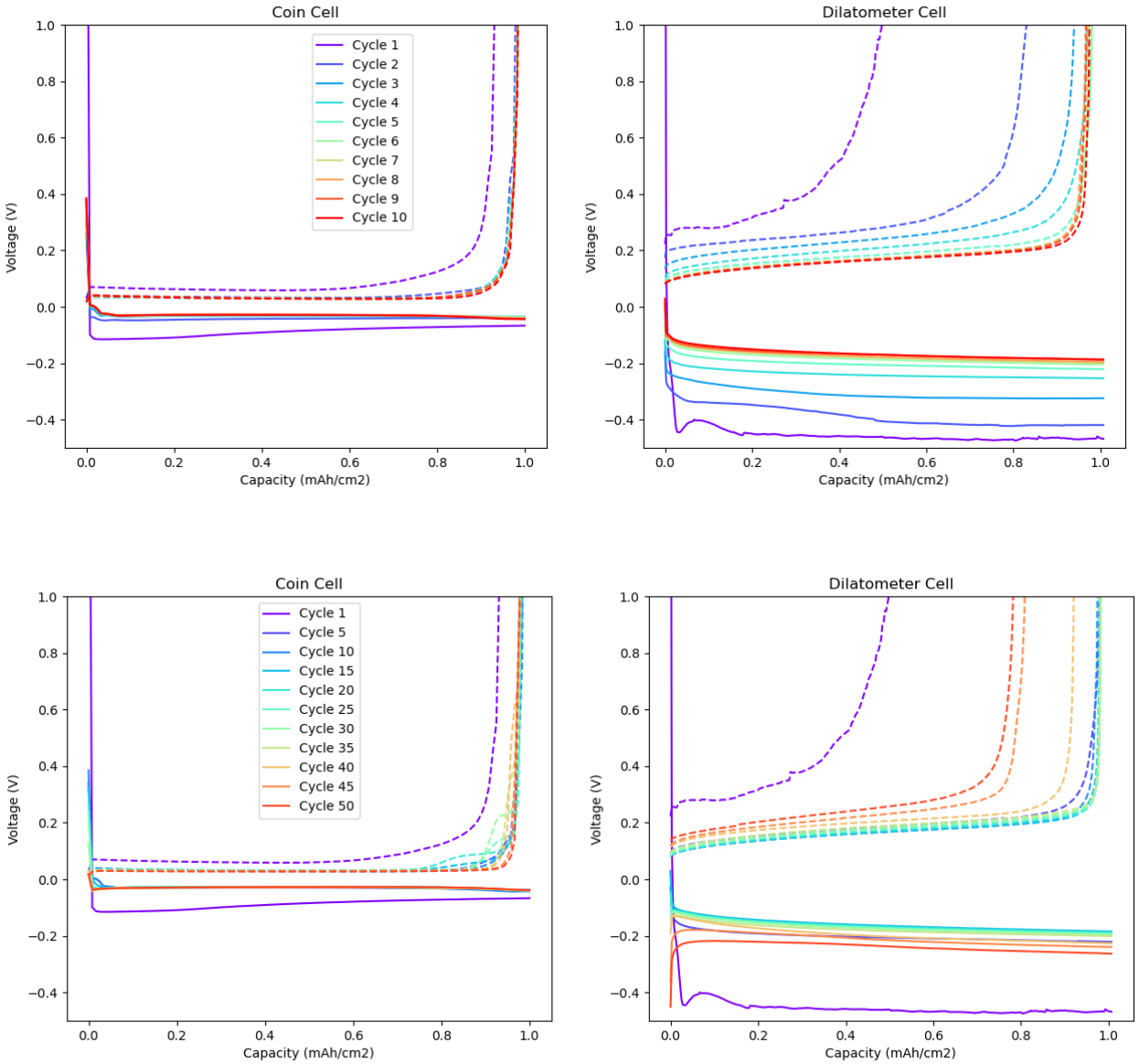


Figure S4: Voltage vs. capacity curves for (top) the first 10 cycles of Li cycling and (bottom) select cycles from 1-50 on 100 nm Ag at 1 mA/cm^2 for 1 mAh/cm^2 in (left) a coin cell and (right) a dilatometer cell.

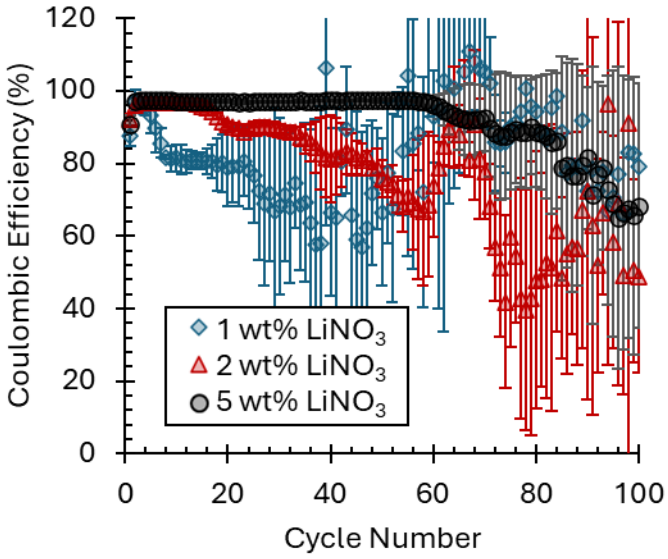


Figure S5: Cycle number vs. Coulombic efficiency for Li cycling on a Cu substrate at 1 mA/cm^2 for 1 mAh/cm^2 in 1 M LiTFSI in DOL:DME (50:50 v:v) with varying concentrations of $LiNO_3$.

Table S1: Alloying reactions and corresponding voltages reported for Ag and Au substrates.

Substrate	Product	Reaction	E vs. Li^+/Li^0 [V]	Reference
Au	LiAu	$Au + Li^+ + e^- \rightarrow LiAu$	0.215	[1-3]
	Li_3Au	$LiAu + 2Li^+ + 2e^- \rightarrow Li_3Au$	0.134	
	Li	$Li^+ + e^- \rightarrow Li$	0	
Ag	LiAg	$Ag + Li^+ + e^- \rightarrow LiAg$	0.23	[4-7]
	Li_9Ag_4	$4LiAg + 5Li^+ + 5e^- \rightarrow Li_9Ag_4$	0.121	
	Li_4Ag	$Li_9Ag_4 + 7Li^+ + 7e^- \rightarrow 4Li_4Ag$	0.091	
	Li_9Ag	$Li_4Ag + 5Li^+ + 5e^- \rightarrow Li_9Ag$	0.03	
	Li	$Li^+ + e^- \rightarrow Li$	0	

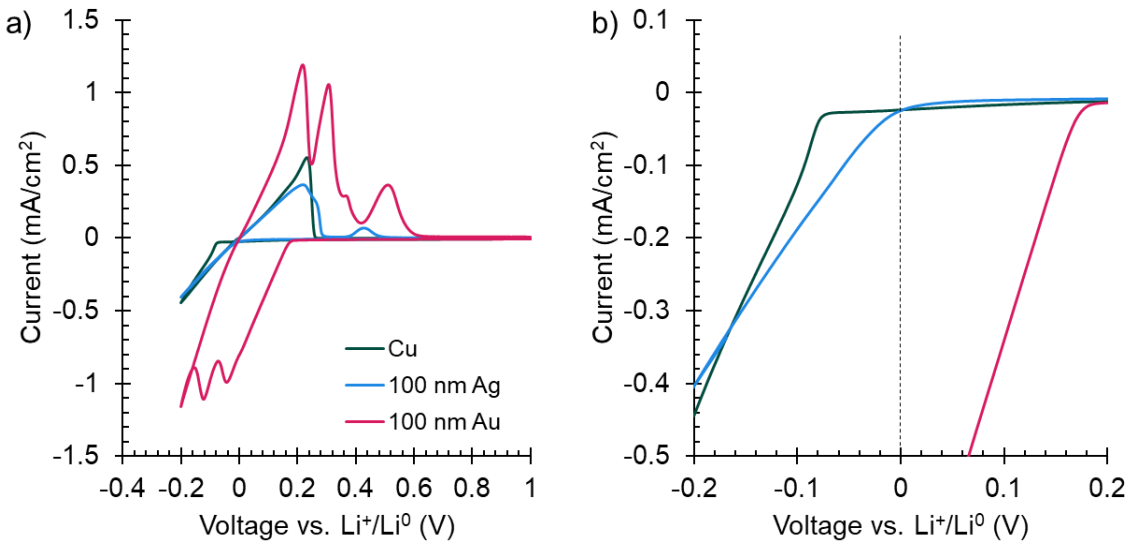


Figure S6: (a) CV of 1 M LiTFSI in DOL:DME with 5 wt% $LiNO_3$ with Cu (green), 100 nm Ag (blue), and 100 nm Au (pink) working electrodes. (b) enlarged portion of CV showing onset of reduction current for each substrate. Scan rate was 1 mV/s.

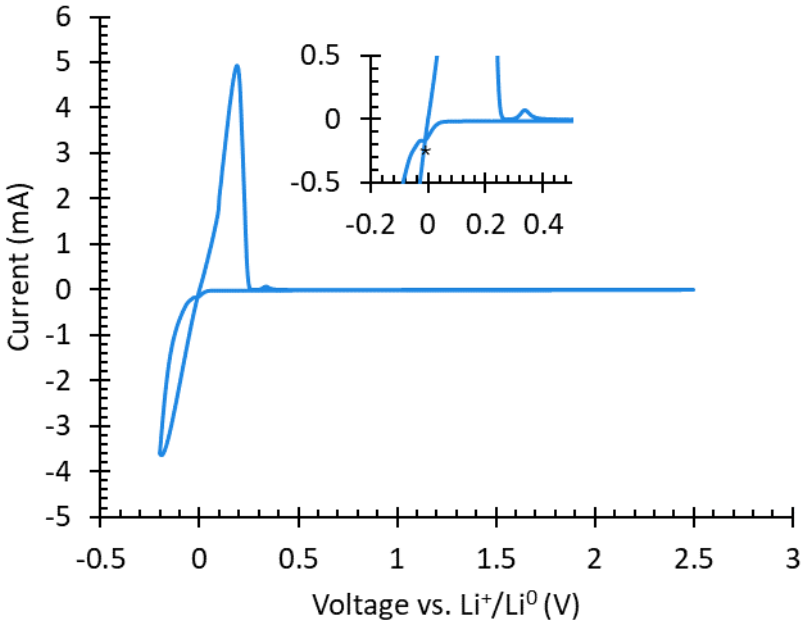


Figure S7: (a) CV of 1 M LiTFSI in DOL:DME with 5 wt% $LiNO_3$ with 100 nm Ag working electrode at scan rate of 0.1 mV/s. Inset shows enlarged portion of CV with asterisk (*) indicating peak associated with Li-Ag alloying.

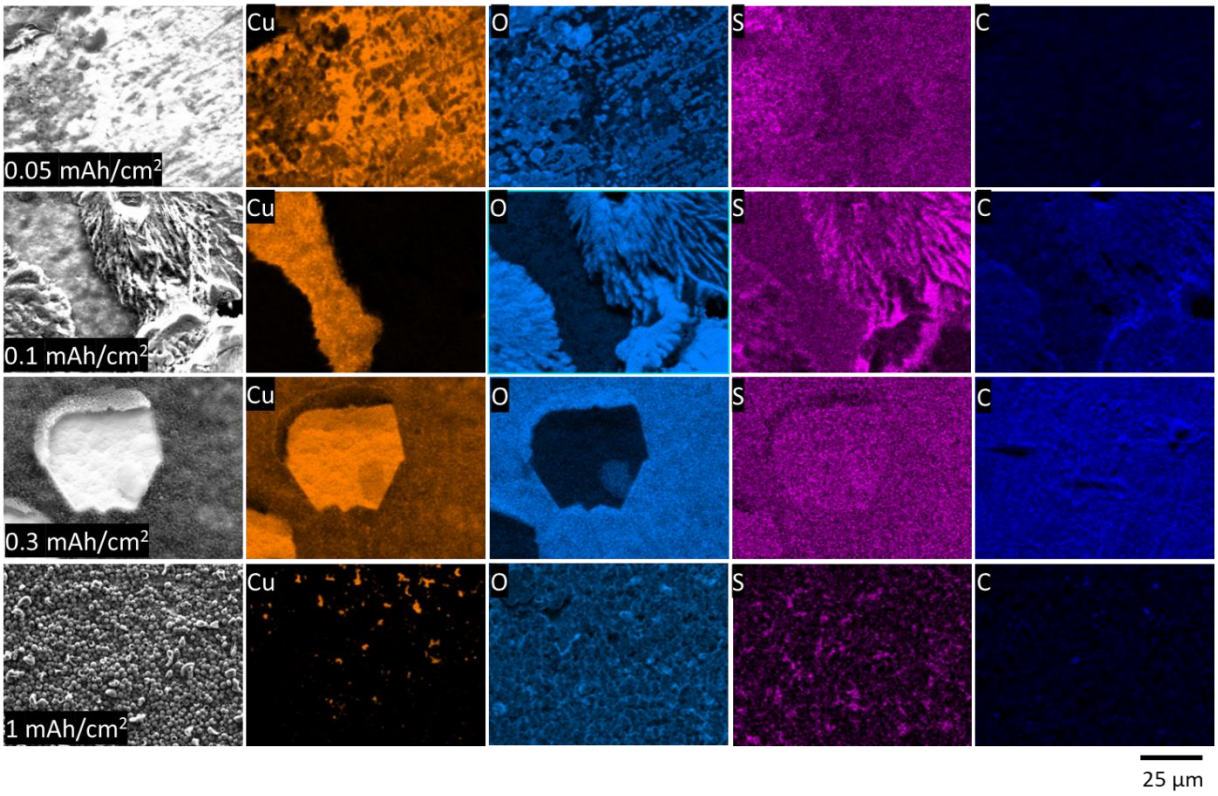


Figure S8: SEM image and corresponding element EDS maps for Li deposited on Cu at 1 mA/cm^2 for 0.05, 0.1, 0.3, and 1 mAh/cm^2. The EDS mapping was completed on the same samples as shown in Figure 1 but may be from different points on the sample.

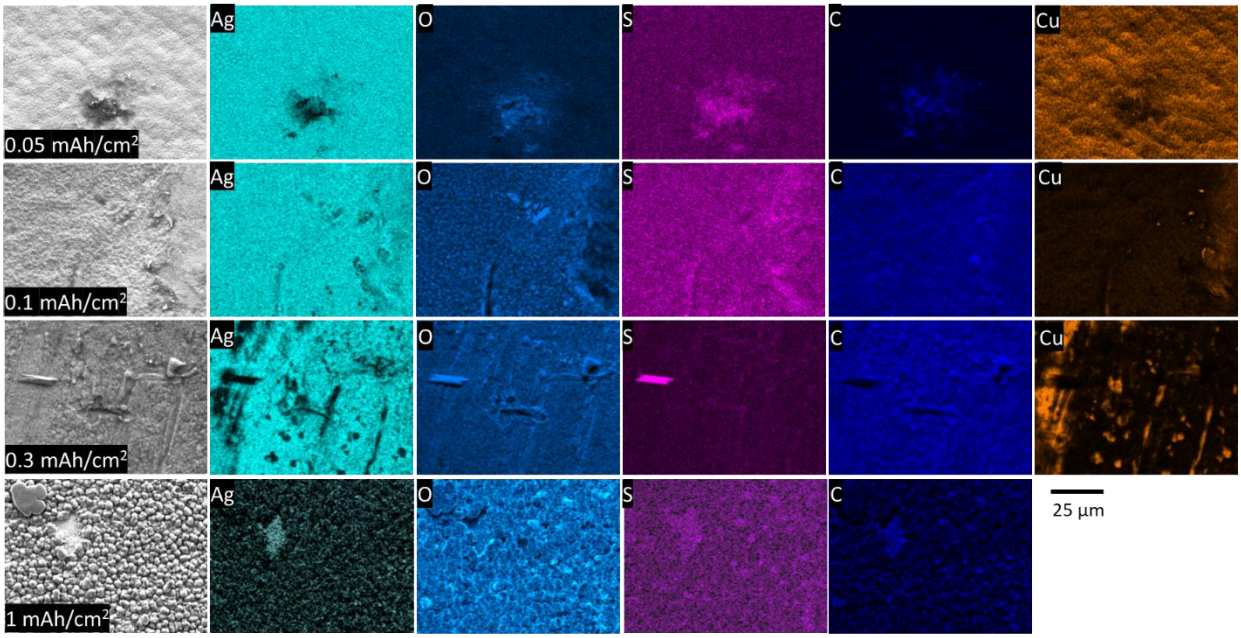


Figure S9: SEM image and corresponding element EDS maps for Li deposited on 100 nm Ag at 1 mA/cm^2 for 0.05, 0.1, 0.3, and 1 mAh/cm^2. The EDS mapping was completed on the same samples as shown in Figure 1 but may be from different points on the sample.

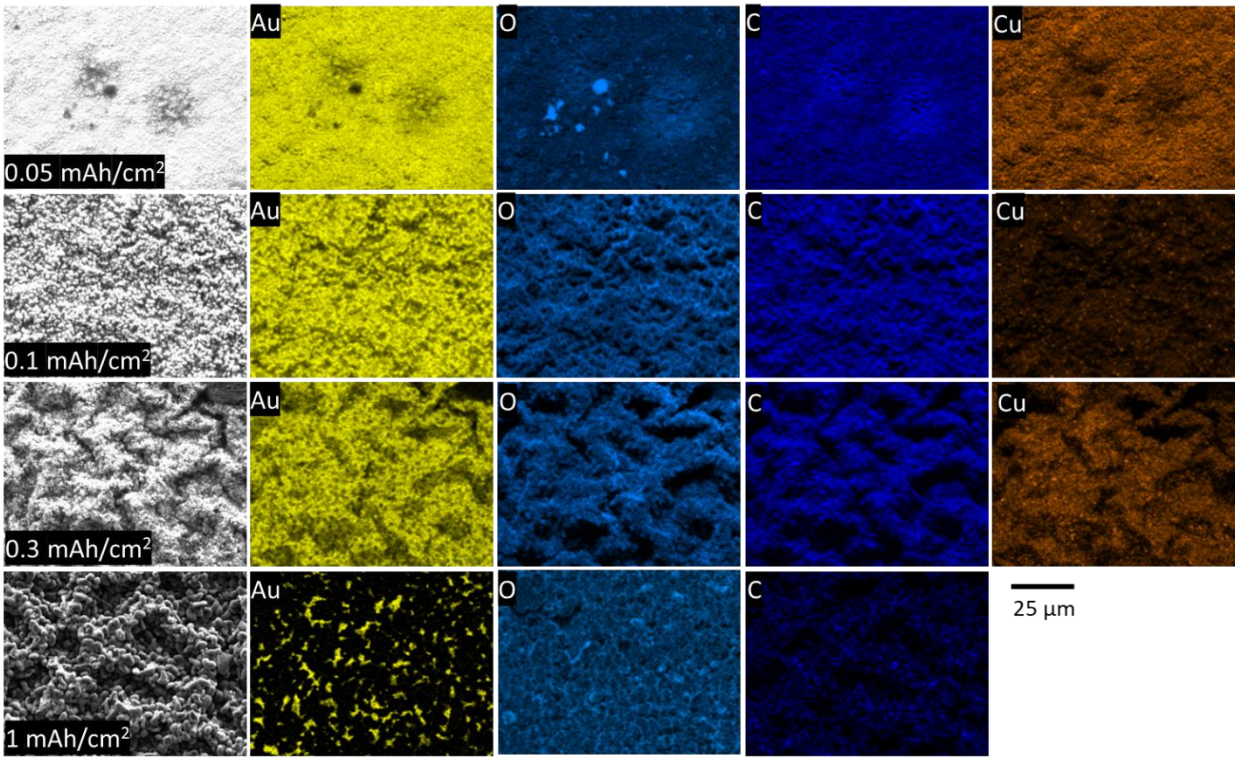


Figure S10: SEM image and corresponding element EDS maps for Li deposited on 100 nm Au at 1 mA/cm^2 for 0.05, 0.1, 0.3, and 1 mAh/cm^2. The EDS mapping was completed on the same samples as shown in Figure 1 but may be from different points on the sample.

Table S2: Estimated capacities for complete lithiation for different Au and Ag lithiated states.

Substrate	Thickness	Lithiated Form	Capacity to Complete Lithiation mAh/cm^2
Au	100	Li_3Au	0.0713
Au	500	Li_3Au	0.357
Au	100	$Li_{15}Au_4$	0.435
Au	500	$Li_{15}Au_4$	0.0871
Ag	100	Li_9Ag	0.0976
Ag	500	Li_9Ag	0.488
Ag	100	$Li_{20}Ag$	0.168
Ag	500	$Li_{20}Ag$	0.838

Table S3: Average particle size of Li electrodeposits measured from the SEM images shown in Figure 3 and Figure 2.

	1 mA/cm^2			0.1 mA/cm^2		
	Cu	100 nm Ag	100 nm Au	Cu	100 nm Ag	100 nm Au
Particle diameter/ length (μm)	0.528 ± 0.12	1.135 ± 0.26	1.216 ± 0.31	5.095 ± 1.1	5.327 ± 1.1	4.850 ± 0.87

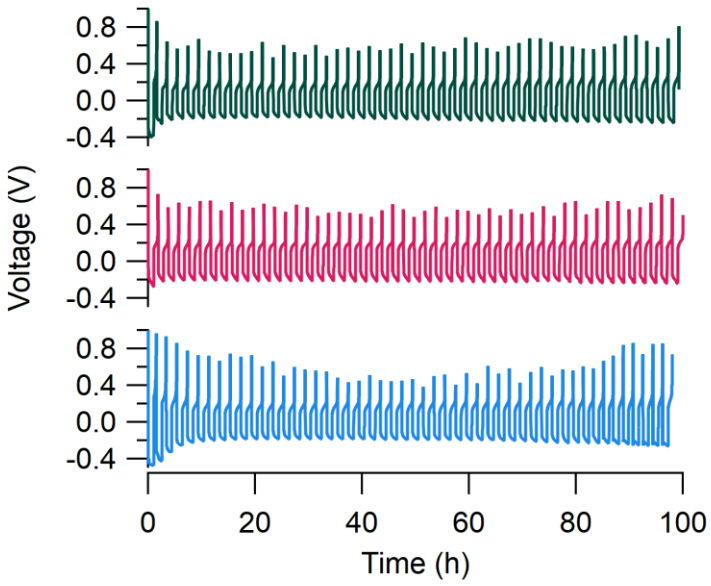


Figure S11: Voltage vs time graphs for dilatometer data from Figure 2. Li was cycled onto Cu (green), 100 nm Au (pink), and 100 nm Ag (blue) substrates at 1 mA/cm^2 for 1 mAh/cm^2.

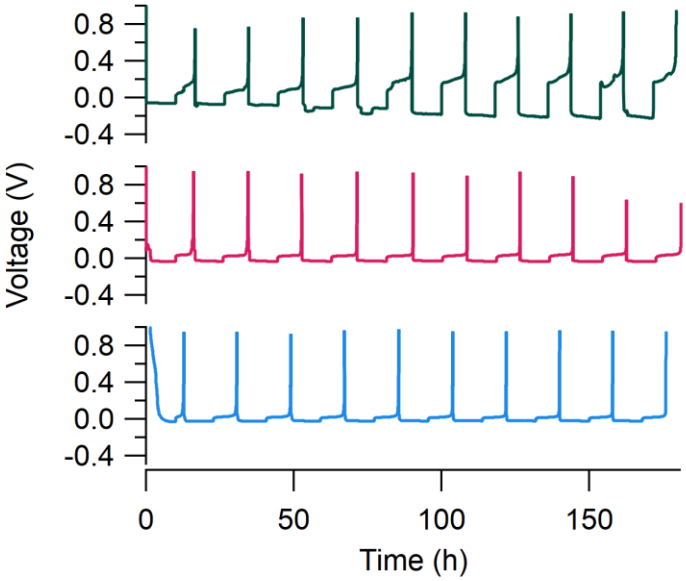


Figure S12: Voltage vs time graphs for dilatometer data from Figure 4. Li was cycled onto Cu (green), 100 nm Au (pink), and 100 nm Ag (blue) substrates at 0.1 mA/cm^2 for 1 mAh/cm^2.

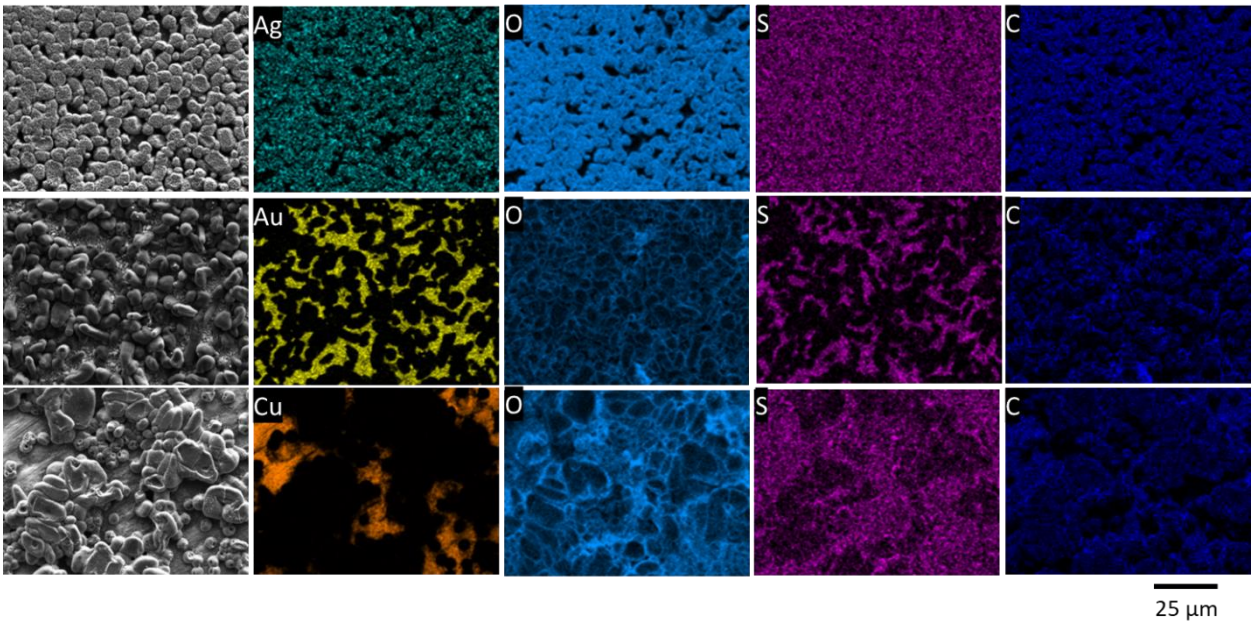


Figure S13: SEM image and corresponding element EDS maps for Li deposited on 100 nm Ag (top), 100 nm Au (middle), and Cu (bottom) at 0.1 mA/cm^2 for 1 mAh/cm^2. The EDS mapping was completed on the same samples as shown in Figure 3 but may be from different points on the sample.

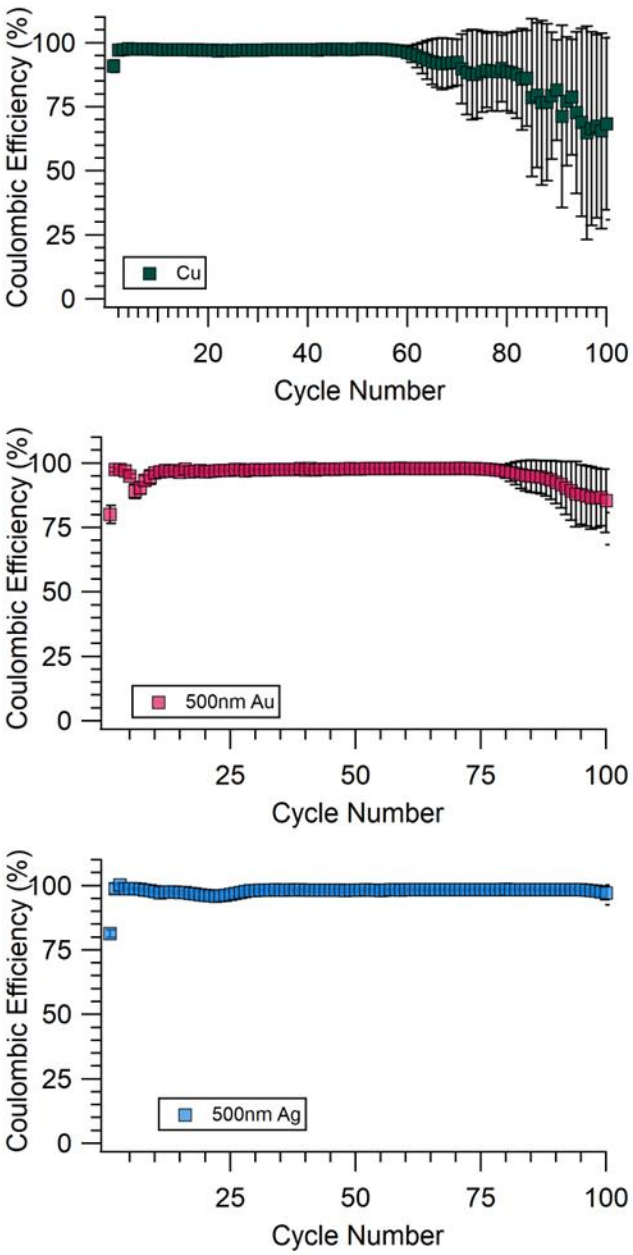


Figure S14: Extended cycling for Li on Cu (top), 500 nm Au (middle), and 500 nm Ag (bottom) substrates in 1 M LiTFSI in DOL:DME with 5 wt% $LiNO_3$. Averages are representative of at least 3 cells with error bars representing the standard deviation. Cells were cycled at 1 mA/cm^2 for 1 mAh/cm^2.

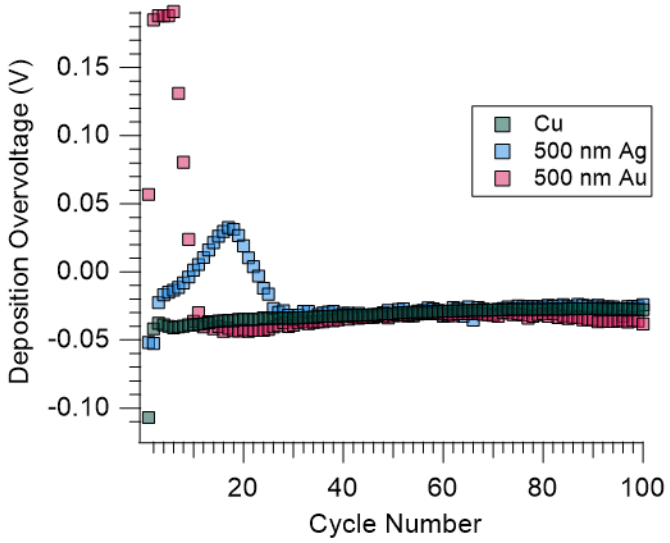


Figure S15: Deposition overvoltage vs cycle number from representative coin cells from Figure 5 and Figure S14. Deposition overvoltage was taken from the voltage when current is first applied on each cycle.

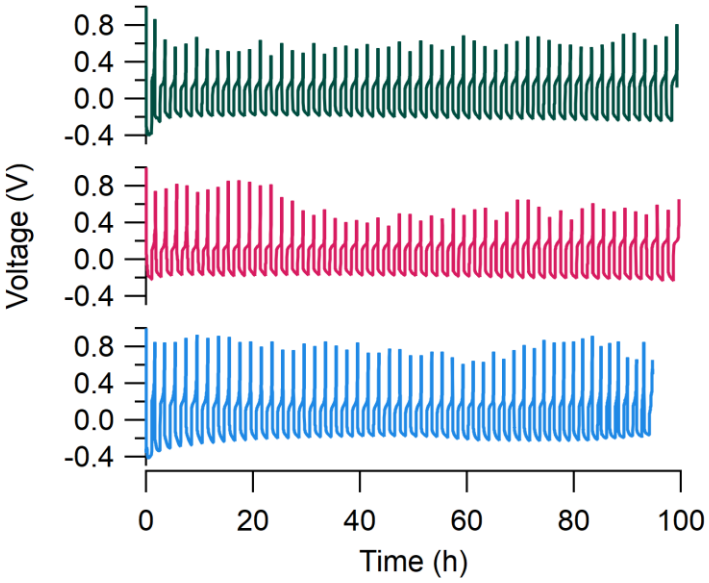


Figure S16: Voltage vs time graphs for dilatometer data from Figure 5. Li was cycled onto Cu (green), 500 nm Au (pink), and 500 nm Ag (blue) substrates at 1 mA/cm^2 for 1 mAh/cm^2.

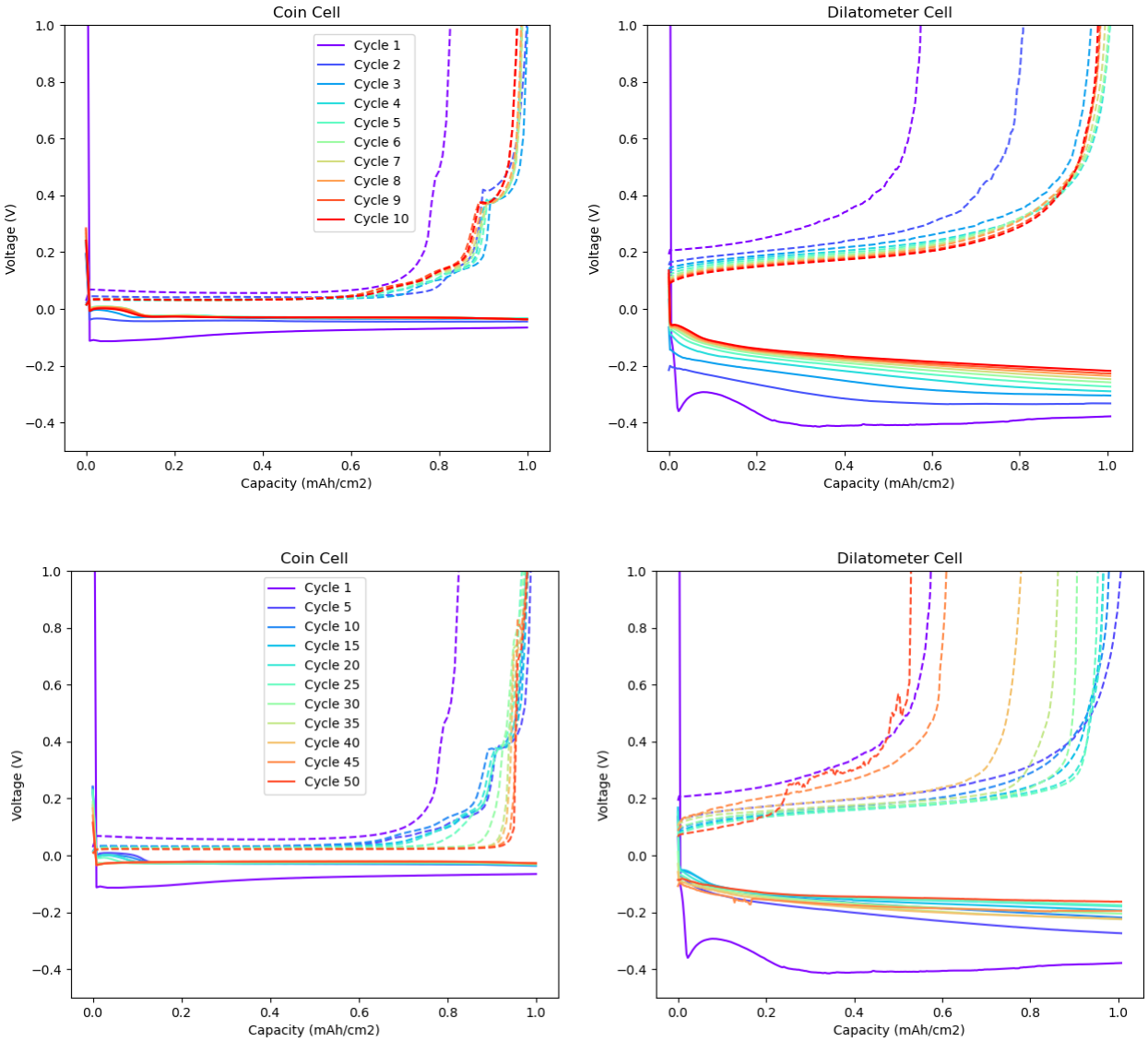


Figure S17: Voltage vs. capacity curves for (top) the first 10 cycles and (bottom) select cycles from 1-50 of Li cycling on 500 nm Ag at 1 mA/cm^2 for 1 mAh/cm^2 in (left) a coin cell and (right) a dilatometer cell.

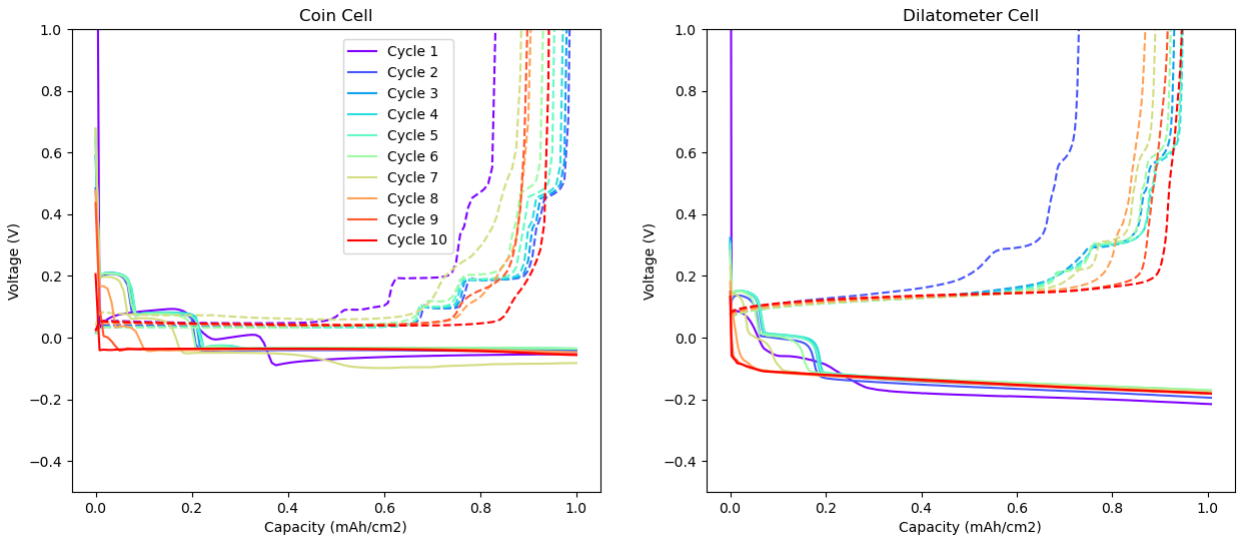


Figure S18: Voltage vs. capacity curves for the first 10 cycles of Li cycling on 500 nm Au at 1 mA/cm^2 for 1 mAh/cm^2 in (left) a coin cell and (right) a dilatometer cell.

Table S4: Average Coulombic efficiencies calculated for different portions of cycling and throughout all 100 cycles for the different substrates evaluated in this study. Averages are calculated from a minimum of 3 replicate cells.

	Average Coulombic Efficiency (%)				
Coating	*100 nm Ag*	*500 nm Ag*	*100 nm Au*	*500 nm Au*	*Cu*
Cycle 1-25	97.99±1.2	96.35±3.19	96.45±1.1	95.40±3.8	97.04±1.3
Cycle 26-50	98.07±0.11	98.12±0.64	97.50±0.22	97.56±0.20	97.34±0.14
Cycle 51-75	98.31±0.062	98.31±0.056	89.19±3.7	97.91±0.074	93.84±3.5
Cycle 76-100	92.98±15	97.77±0.97	78.27±8.1	92.56±4.2	78.73±8.6
Cycle 1-100	96.84±7.6	97.64±1.8	90.35±8.9	95.85±3.5	91.74±8.9

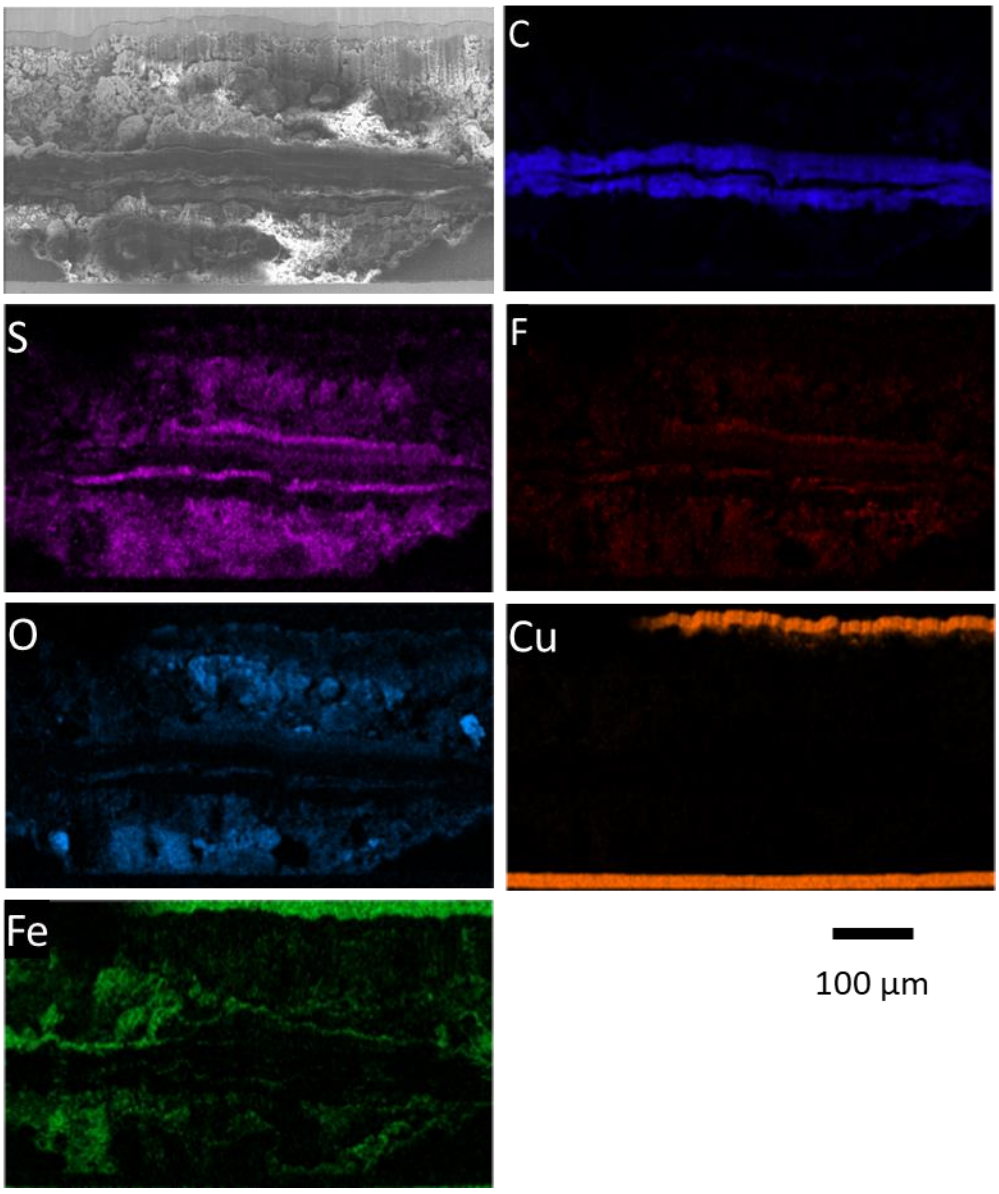


Figure S19: EDS of cross-sectional image of 51st electrodeposition of Li on Cu with 1 M LiTFSI in DOL:DME with 5 wt% $LiNO_3$. Li was cycled at 1 mA/cm^2 for 1 mAh/cm^2.

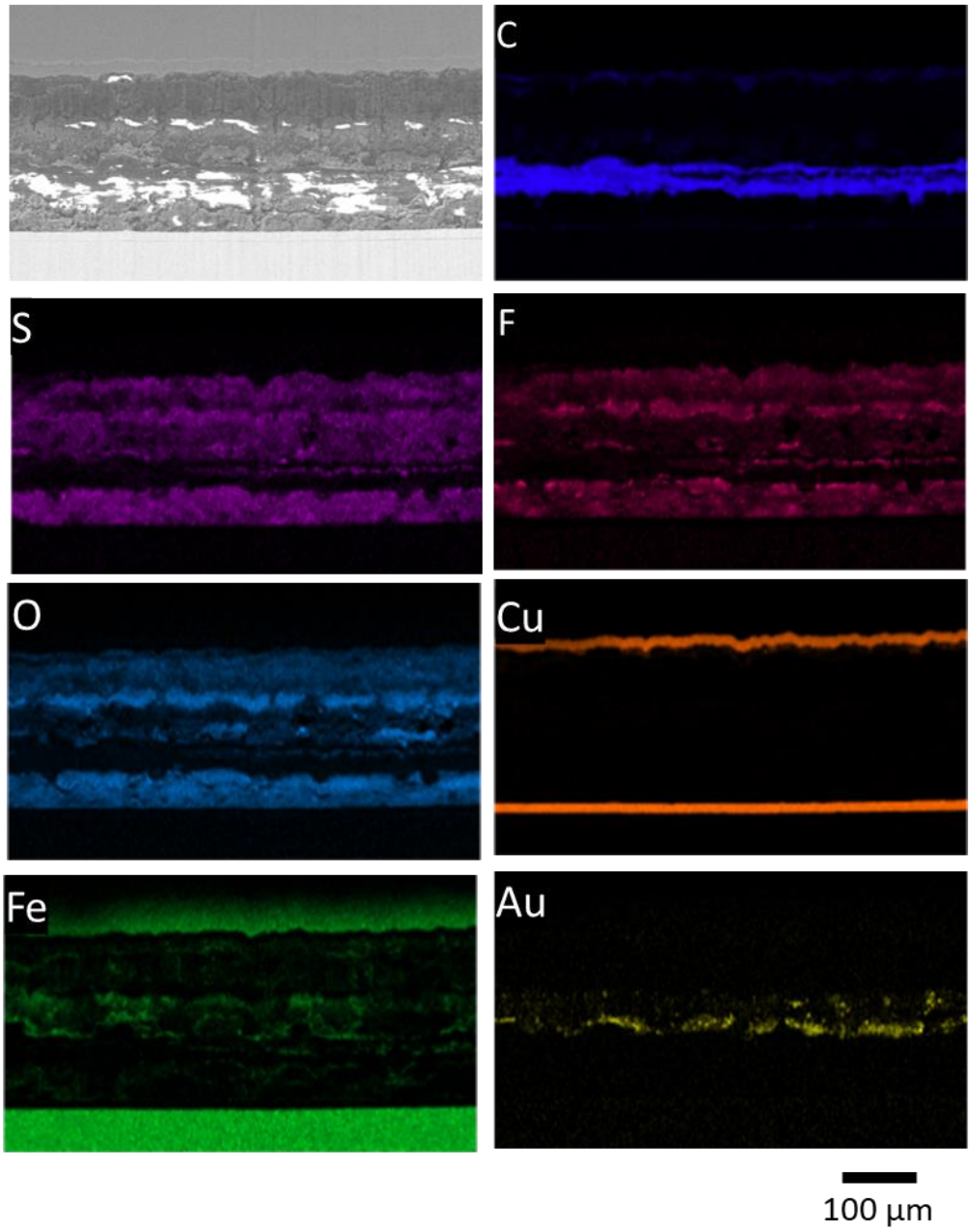


Figure S20: EDS of cross-sectional image of 51st electrodeposition of Li on 500 nm Au with 1 M LiTFSI in DOL:DME with 5 wt% $LiNO_3$. Li was cycled at 1 mA/cm^2 for 1 mAh/cm^2.

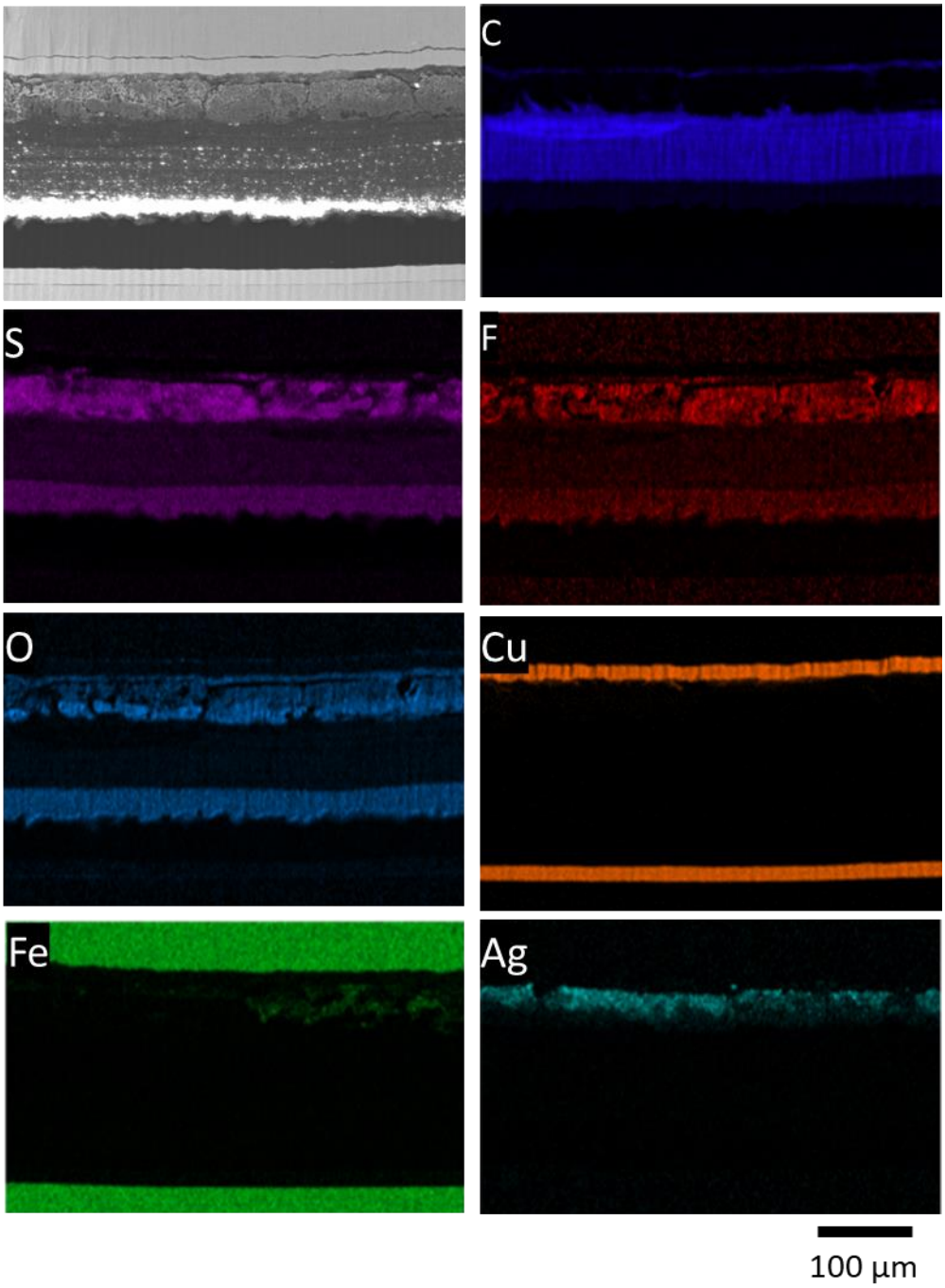


Figure S21: EDS of cross-sectional image of 51st electrodeposition of Li on 500 nm Ag with 1 M LiTFSI in DOL:DME with 5 wt% $LiNO_3$. Li was cycled at 1 mA/cm^2 for 1 mAh/cm^2.

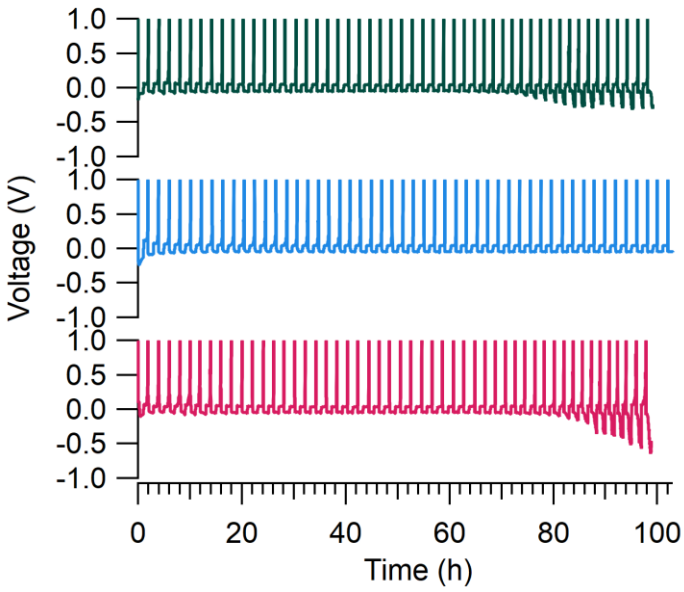


Figure S22: Voltage vs time curves for 51 electrodeposition cycles for laser PFIB cross sectional images shown in Figure 6. Top (green) trace is Cu, middle (blue) trace is 500 nm Ag, and bottom (pink) trace is 500 nm Au.

Acknowledgments: We thank Bryan Wygant for useful discussions and feedback, Ben Warren for general laboratory support, and Ken Coombes and Steven Larson for assistance with the deposition of the metals. Sandia National Laboratories is a multimission laboratory managed and operated by National Technology & Engineering Solutions of Sandia, LLC, a wholly owned subsidiary of Honeywell International Inc., for the U.S. Department of Energy's National Nuclear Security Administration under contract DE-NA0003525. This paper describes objective technical results and analysis. Any subjective views or opinions that might be expressed in the paper do not necessarily represent the views of the U.S. Department of Energy or the United States Government. This article has been authored by an employee of National Technology & Engineering Solutions of Sandia, LLC under Contract No. DE-NA0003525 with the U.S. Department of Energy (DOE). The employee owns all right, title and interest in and to the article and is solely responsible for its contents. The United States Government retains and the publisher, by accepting the article for publication, acknowledges that the United States Government retains a non-exclusive, paid-up, irrevocable, world-wide license to publish or reproduce the published form of this article or allow others to do so, for United States Government purposes. The DOE will provide public access to these results of federally sponsored research in accordance with the DOE Public Access Plan https://www.energy.gov/downloads/doe-public-access-plan.

References:

[1] J. Hertle, F. Walther, B. Mogwitz, S. Schroder, H. Richter, and J. Janek, "Miniaturization of Reference Electrodes for Solid-State Lithium-Ion Batteries," *Journal of The Electrochemical Society,* vol. 170, p. 040519, 2023, doi: 10.1149/1945-7111/accb6f.

[2] P. Bach, M. Stratmann, I. Valencia-Jaime, A. H. Romero, and F. U. Renner, "Lithiation and Delithiation Mechanisms of Gold Thin Film Model Anodes for Lithium Ion Batteries: Electrochemical Characterization," *Electrochimica Acta,* vol. 164, no. 81-89, 2015, doi: 10.1016/j.electacta.2015.02.184.

[3] T. L. Kulova, A. M. Skundin, V. M. Kozhevin, D. A. Yavsin, and S. A. Gurevich, "A Study of Lithium Insertion into Electrodes with Thin Gold Films," *Russian Journal of Electrochemistry,* vol. 46, no. 8, pp. 877-881, 2010, doi: 10.1134/S1023193510080033.

[4] Y. Huang *et al.*, "Unlocking the Potential of Li-Ag Alloys: Phase Selection and Practical Application," *Energy Material Advances,* vol. 5, pp. 1-10, 2024, doi: 10.34133/energymatadv.0108.

[5] S. Jin *et al.*, "Solid–Solution-Based Metal Alloy Phase for Highly Reversible Lithium Metal Anode," *Journal of the American Chemical Society,* vol. 142, no. 19, pp. 8818-8826, 2020, doi: 10.1021/jacs.0c01811.

[6] G. Taillades and J. Sarradin, "Silver: high perfromance anode for thin film lithium ion batteries," *Journal of Power Sources,* vol. 125, no. 2, pp. 199-205, 2004, doi: 10.1016/j.jpowsour.2003.07.004.

[7] J. Thomas, S. S. Behara, and A. Van der Ven, "Thermodynamic and Kinetic Properties of the Lithium-Silver System," *Chemistry of Materials,* vol. 36, no. 18, pp. 8936-8948, 2024, doi: 10.1021/acs.chemmater.4c01903.